ISPRS Journal of Photogrammetry and Remote Sensing 84 (2013) 43–51

Contents lists available at SciVerse ScienceDirect

ISPRS Journal of Photogrammetry and Remote Sensing

journal homepage: www.elsevier.com/locate/isprsjprs

# Direct georeferencing of airborne LiDAR data in national coordinates

Yongjun Zhang *, Xiang Shen

*School of Remote Sensing and Information Engineering, Wuhan University, No. 129 Luoyu Road, Wuhan 430079, PR China*

ARTICLE INFO

*Article history:*
Received 21 February 2013
Received in revised form 4 July 2013
Accepted 4 July 2013

*Keywords:*
Distortion
Georeferencing
Laser scanning
Map projection
Position and orientation system (POS)

ABSTRACT

The topographic mapping products of airborne light detection and ranging (LiDAR) are usually required in the national coordinates (i.e., using the national datum and a conformal map projection). Since the spatial scale of the national datum is usually slightly different from the World Geodetic System 1984 (WGS 84) datum, and the map projection frame is not Cartesian, the georeferencing process in the national coordinates is inevitably affected by various geometric distortions. In this paper, all the major direct georeferencing distortion factors in the national coordinates, including one 3D scale distortion (the datum scale factor distortion), one height distortion (the earth curvature distortion), two length distortions (the horizontal-to-geodesic length distortion and the geodesic-to-projected length distortion), and three angle distortions (the skew-normal distortion, the normal-section-to-geodesic distortion, and the arc-to-chord distortion) are identified and demonstrated in detail; and high-precision map projection correction formulas are provided for the direct georeferencing of the airborne LiDAR data. Given the high computational complexity of the high-precision map projection correction approach, some more approximate correction formulas are also derived for the practical calculations. The simulated experiments show that the magnitude of the datum scale distortion can reach several centimeters to decimeters for the low (e.g., 500 m) and high (e.g., 8000 m) flying heights, and therefore it always needs to be corrected. Our proposed practical map projection correction approach has better accuracy than Legat's approach,[1] but it needs 25% more computational cost. As the correction accuracy of Legat's approach can meet the requirements of airborne LiDAR data with low and medium flight height (up to 3000 m above ground), our practical correction approach is more suitable to the high-altitude aerial imagery. The residuals of our proposed high-precision map projection correction approach are trivial even for the high flight height of 8000 m. It can be used for the theoretical applications such as the accurate evaluation of different GPS/INS attitude transformation methods to the national coordinates.



## 1. Introduction

In the field of aerial topographic survey, georeferencing commonly involves two consecutive procedures: sensor orientation and scene restitution (Legat, 2006). The former process aims to precisely acquire the exterior orientation parameters (EOPs) of the imaging sensor, and the latter process aims to calculate the ground coordinates by combining the EOPs and the imaging sensor observations (e.g., the ranges and the scan angles in airborne laser scanning and the image coordinates in aerial imagery). Benefiting from the emergence and continuous improvement of high performance navigation sensors and the GPS/INS integrated navigation algorithm, high-precision EOPs can be reliably acquired by the airborne position and orientation system (POS), which can be directly applied to the subsequent scene restitution procedure. This data processing approach is generally referred to as the direct georeferencing (DG) method (Skaloud, 2002). The data processing flow is greatly simplified because the measurements of ground control points (GCPs) and the least-squares adjustment are not required in the DG process, unlike the traditional indirect georeferencing method (Habib et al., 2006; Ressl, 2001) and the integrated georeferencing method (also known as integrated sensor orientation, however, this term is not preferred in this paper because it does not literally cover the content of the scene restitution procedure) (Blázquez and Colomina, 2012; Ip et al., 2007; Khoshelham, 2009). However, in the scene restitution procedure of the DG approach, the ground points are extrapolated from the imaging sensor center (Yastikli and Jacobsen, 2005); and without the constraints of the GCPs and tie points (TPs), it is very sensitive to any source of systematic and random errors.

Aerial photogrammetry and laser scanning data products, such as digital terrain models (DTMs) and orthoimages, are usually required in the national coordinates (i.e., using the national geodetic datum and the conformal map projection) (Legat, 2006; Ressl,

* Corresponding author.
*E-mail addresses:* zhangyj@whu.edu.cn (Y. Zhang), shen@whu.edu.cn (X. Shen).

[1] Legat (2006).

0924-2716/$ - see front matter © 2013 International Society for Photogrammetry and Remote Sensing, Inc. (ISPRS) Published by Elsevier B.V. All rights reserved.
http://dx.doi.org/10.1016/j.isprsjprs.2013.07.003

2001). However, direct georeferencing in the national coordinates is unavoidably influenced by a variety of geometric distortions because the spatial scale of the national datum is usually slightly different from World Geodetic System 1984 (WGS 84) datum, and the map projection frame is not a Cartesian frame. For the special case of airborne light detection and ranging (LiDAR), two options are available to address this issue (Legat, 2006). The first approach is to bypass the problem by first choosing a suitable Cartesian frame of the WGS 84 datum for the process of sensor orientation and scene restitution, converting the georeferencing results (i.e., the ground points) then to the geodetic coordinates of the national datum, and finally transforming them into the required national map projection frame individually by using the map projection formula. This method is quite accurate because the transformation errors of the commonly used map projection formulas are usually negligible for the aerial topographic survey. The second approach is more straightforward as it directly chooses the national map projection frame for the direct georeferencing process and compensates for the spatial scale distortion and the map projection distortions as much as possible, which is the main focus of this paper.

To the best of our knowledge, there are no studies that have investigated the effect of the spatial scale distortion on the DG process in the national datum. On the other hand, correcting the map projection distortions is a very long-standing topic in the aerial photogrammetry field. All the early studies focused on earth curvature correction (Hothmer, 1958; Wang, 1980), and distortion correction already has been well implemented in the available aerial photogrammetry software. In recent years, length distortion has received increasing attention because it severely impairs direct georeferencing accuracy. Several length correction algorithms have been developed and evaluated for the direct georeferencing process of airborne LiDAR data (Legat, 2006) or aerial imagery (Legat, 2006; Ressl, 2001; Yastikli and Jacobsen, 2005); and both simulated data (Legat, 2006) and real data (Skaloud and Legat, 2008) experiments proved that they could significantly improve direct georeferencing accuracy. However, the existing correction approaches are still not fully satisfactory for all aerial mapping scenarios. According to the simulated experiments, the residuals are usually significant and come from two sources: (1) the existing earth curvature correction and length correction formulas are not accurate enough; and (2) some small amount of distortion factors have yet to be characterized and quantified.

In this paper, we identify all the major geometric distortion factors by analyzing how to transform a vector from a Cartesian frame of the WGS 84 datum to the national map projection frame; and further, we provide the high-precision map projection correction formulas and the more practical formulas for the direct georeferencing process of the airborne LiDAR data. The remainder of this paper is organized as follows. In Section 2, we first introduce and define five essential reference frames (i.e., the sensor frame, the earth-centered earth-fixed frame, the eccentric earth-fixed frame, the map projection frame, and the local level frame of the national ellipsoid) and further provide the transformation formulas of the EOPs to the last three frames. Then, we present the computational model of the airborne LiDAR data and the concept of the DG vector in the direct georeferencing process. Finally, through the analysis of the transformation procedures of the DG vector from the earth-centered earth-fixed frame to the national map projection frame, we identify and demonstrate all the major geometric distortion factors of the direct georeferencing process in the national coordinates. In Section 3, we derive the high-precision map projection correction formulas based on the equations from the geometric geodesy and provide the practical formulas for reducing the computational efforts. The accuracies and computational costs of different correction approaches are carefully evaluated in the simulated experiments of Section 4; and in the last part of this paper, we present our concluding remarks.

## 2. Geometric basis

### 2.1. Reference frames

The direct georeferencing process involves at least seven to eight different reference frames in the navigation, geodesy, and photogrammetry field. To avoid unnecessary technical details, only five essential frames are introduced in this paper, most of which are schematically shown in Fig. 1. All the reference frames are assumed to be right-handed.

1. Sensor frame (s-frame). In this paper, the imaging sensor refers specifically to the airborne LiDAR. The coordinate origin is the laser emission position, the *X*-axis is assumed to be along the trajectory direction, and the *Z*-axis points upward.
2. Earth-centered earth-fixed frame (e-frame). It refers to the WGS 84 reference frame. The *X*-axis points toward the Greenwich meridian in the equatorial plane, and the *Z*-axis points toward the North Pole.
3. Eccentric earth-fixed frame (e′-frame). This is an earth-fixed frame defined by the national geodetic datum. The coordinate origin is at the center of the national reference ellipsoid, which usually deviates from the mass center of the earth slightly.
4. National map projection frame (p-frame). The coordinate origin is usually the intersection point between the central meridian and the equator (the false east and false north are not considered). The axis directions follow the east-north-up (ENU) convention. It is worth noting that this work only uses the ellipsoidal heights, and the orthometric heights are not treated.
5. Local level frame of the national ellipsoid (l-frame). This frame is mainly used to achieve the rotation between the e′-frame and the p-frame and to facilitate the understanding of the map projection distortions. The coordinate origin is the sensor center, and the axis directions follow the ENU convention. The *X*-axis points east along the tangent of the prime vertical, the *Y*-axis points north along the tangent of the meridian, and the *Z*-axis points upward along the ellipsoidal normal.

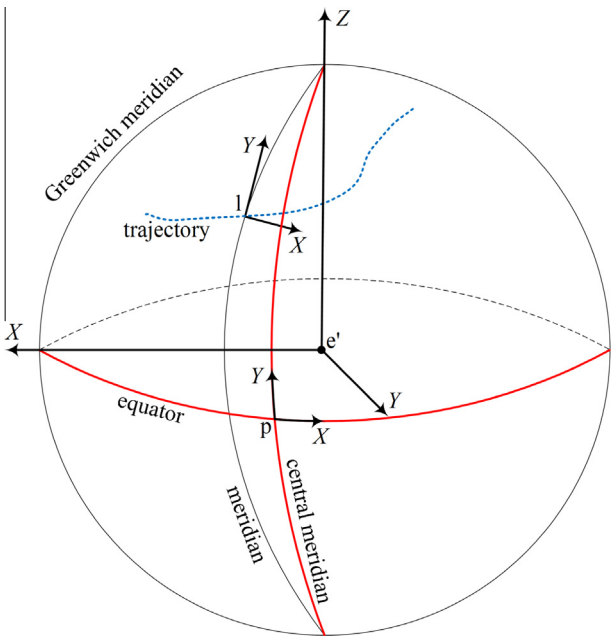


**Fig. 1.** Some reference frames required in direct georeferencing.

### 2.2. Transformation of exterior orientation parameters

Before restituting the scene, the EOPs first should be transformed to the desired reference frames. Without going into detail, this paper assumes that the EOPs are already represented in the e-frame (the transformation process of GPS/INS trajectory to the e-frame can be found in (Bäumker and Heimes, 2002)). The next work is then to transform these EOPs to the e′-frame, l-frame, and p-frame.

#### 2.2.1. Eccentric earth-fixed frame

In national mapping, the geometric relation between two different datums is usually represented by a Helmert 7-parameter transformation (International Association of Oil and Gas Producers, 2013). If we denote the linear EOPs of the e-frame as $\boldsymbol{T}_{\mathrm{s}}^{\mathrm{e}}$ (i.e., the position vector constituted by the sensor center coordinate in the e-frame) and the attitude matrix as $\boldsymbol{R}_{\mathrm{s}}^{\mathrm{e}}$ (i.e., the rotation matrix transformed from the s-frame to the e-frame), then the EOPs in the e′-frame can be expressed by

$$\boldsymbol{T}_{\mathrm{s}}^{\mathrm{e}'} = m\boldsymbol{R}_{\mathrm{e}}^{\mathrm{e}'}\boldsymbol{T}_{\mathrm{s}}^{\mathrm{e}} + \boldsymbol{T}_{\mathrm{e0}}^{\mathrm{e}'} \tag{1}$$

and

$$\boldsymbol{R}_{\mathrm{s}}^{\mathrm{e}'} = \boldsymbol{R}_{\mathrm{e}}^{\mathrm{e}'}\boldsymbol{R}_{\mathrm{s}}^{\mathrm{e}} \tag{2}$$

where $m$ is the datum scale factor, $\boldsymbol{R}_{\mathrm{e}}^{\mathrm{e}'}$ represents the rotation matrix transformed from the e-frame to the e′-frame, and $\boldsymbol{T}_{\mathrm{e0}}^{\mathrm{e}'}$ is the e-frame origin given in the e′-frame.

#### 2.2.2. Local level frame of the national ellipsoid

If we already have the EOPs in the e′-frame, then the EOPs in the l-frame can be given by

$$\boldsymbol{T}_{\mathrm{s}}^{\mathrm{l}} = \boldsymbol{R}_{\mathrm{e}'}^{\mathrm{l}}\left(\boldsymbol{T}_{\mathrm{s}}^{\mathrm{e}'} - \boldsymbol{T}_{\mathrm{l0}}^{\mathrm{e}'}\right) \tag{3}$$

and

$$\boldsymbol{R}_{\mathrm{s}}^{\mathrm{l}} = \boldsymbol{R}_{\mathrm{e}'}^{\mathrm{l}}\boldsymbol{R}_{\mathrm{s}}^{\mathrm{e}'} \tag{4}$$

where $\boldsymbol{R}_{\mathrm{e}'}^{\mathrm{l}}$ represents the rotation matrix transformed from the e′-frame to the l-frame, and $\boldsymbol{T}_{\mathrm{l0}}^{\mathrm{e}'}$ is the l-frame origin coordinate in the e′-frame, which can be given by the conversion result from ellipsoidal to Cartesian (geocentric) coordinate. Their detailed equations (International Association of Oil and Gas Producers, 2013) are

$$\begin{aligned}\boldsymbol{R}_{\mathrm{e}'}^{\mathrm{l}} &= \boldsymbol{R}_X(\pi/2-\varphi)\boldsymbol{R}_Z(\pi/2+\lambda)\\ &= \begin{bmatrix} -\sin\lambda & \cos\lambda & 0\\ -\sin\varphi\cos\lambda & -\sin\varphi\sin\lambda & \cos\varphi\\ \cos\varphi\cos\lambda & \cos\varphi\sin\lambda & \sin\varphi\end{bmatrix}\end{aligned}$$

and

$$\boldsymbol{T}_{\mathrm{l0}}^{\mathrm{e}'} = \begin{bmatrix}(\upsilon+h)\cos\varphi\cos\lambda\\ (\upsilon+h)\cos\varphi\sin\lambda\\ (\upsilon-e^2\upsilon+h)\sin\varphi\end{bmatrix} \tag{6}$$

respectively, where the subscripts $X$ and $Z$ mean that the matrix is only rotated by the specific axis; $\varphi$, $\lambda$, $\upsilon$, and $h$ are the geodetic latitude, the geodetic longitude, the curvature radius in the prime vertical plane, and the ellipsoidal height of the sensor center in the national ellipsoid, respectively; and $e$ is the first eccentricity of the national ellipsoid.

#### 2.2.3. National map projection frame

The transformation process of the linear EOPs from the e′-frame to the p-frame needs two consecutive procedures. The geocentric coordinates of the e′-frame are first transformed to the ellipsoidal coordinates, and then they are projected to the desired p-frame. The detailed formulas are dependent on the specific map projection used, and some of the frequently-used coordinate conversion formulas have been published by the International Association of Oil and Gas Producers (2013).

As for the angular EOPs, note that both the $Z$-axes of the l-frame and p-frame point upward along the ellipsoidal normal, but their $Y$-axes point toward true north and grid north (cf. Fig. 2), respectively. The angular difference is the grid convergence $\gamma$. Therefore,

$$\boldsymbol{R}_{\mathrm{l}}^{\mathrm{p}} = \begin{bmatrix}\cos\gamma & -\sin\gamma & 0\\ \sin\gamma & \cos\gamma & 0\\ 0 & 0 & 1\end{bmatrix} \tag{7}$$

For the transverse Mercator projection, $\gamma$ can be calculated by (Redfearn, 1948)

$$\begin{aligned}\gamma &= (\lambda-\lambda_0)\sin\varphi + \frac{1}{3}(\lambda-\lambda_0)^3\sin\varphi\cos^2\varphi(2\psi^2-\psi)\\ &+ \frac{1}{15}(\lambda-\lambda_0)^5\sin\varphi\cos^4\varphi[\psi^4(11-24t^2)-\psi^3(11-36t^2)\\ &+ 2\psi^2(1-7t^2)+\psi t^2] + \frac{1}{315}(\lambda-\lambda_0)^7\sin\varphi\cos^6\\ &\varphi(17-26t^2+2t^4)\end{aligned} \tag{8}$$

with $t = \tan\varphi$ and $\psi = \upsilon/\rho$, where $\rho$ is the curvature radius of the national ellipsoid in the meridian plane, and $\lambda_0$ is the geodetic longitude of the central meridian. Consequently, we can obtain

$$\boldsymbol{R}_{\mathrm{s}}^{\mathrm{p}} = \boldsymbol{R}_{\mathrm{l}}^{\mathrm{p}}\boldsymbol{R}_{\mathrm{s}}^{\mathrm{l}} \tag{9}$$

### 2.3. Direct georeferencing model of airborne LiDAR

Theoretically, the direct georeferencing process of the airborne LiDAR data in the e-frame can be abstracted to

$$\boldsymbol{T}_{\mathrm{grd}} = \boldsymbol{T}_{\mathrm{eo}} + \boldsymbol{R}_{\mathrm{eo}}\boldsymbol{R}_{\mathrm{scan}}\boldsymbol{T}_{\mathrm{range}} = \boldsymbol{T}_{\mathrm{eo}} + \boldsymbol{T}_{\mathrm{dg}} \tag{10}$$

where $\boldsymbol{T}_{\mathrm{grd}}$ is the vector constituted by the ground coordinate, $\boldsymbol{T}_{\mathrm{eo}}$ and $\boldsymbol{R}_{\mathrm{eo}}$ are the vector and rotation matrix formed by the linear and angular EOPs, respectively, $\boldsymbol{T}_{\mathrm{range}}$ and $\boldsymbol{R}_{\mathrm{scan}}$ are the range vector and the scan angle matrix, respectively, and $\boldsymbol{T}_{\mathrm{dg}}$ is referred to as the DG vector, which can be calculated by combining the angular EOPs and the laser scanning observations (i.e., the scan angle and the range observation). It can be seen from Eq. (10) that the direct

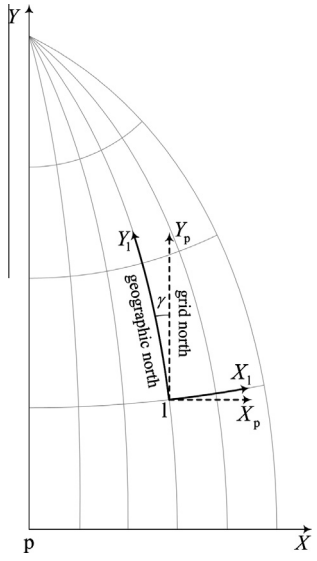


**Fig. 2.** Grid convergence $\gamma$.

georeferencing process of the airborne LiDAR data can be simply expressed as the vector addition operation between $\boldsymbol{T}_{eo}$ and $\boldsymbol{T}_{dg}$.

If direct georeferencing is performed in the p-frame, then $\boldsymbol{T}^{p}_{eo}$ can be accurately calculated by the map projection formula, but $\boldsymbol{T}^{p}_{dg}$ (i.e., the multiplication result of $\boldsymbol{R}^{p}_{eo}\boldsymbol{R}_{scan}\boldsymbol{T}_{range}$) is incorrect because the datum scale is changed and the spatial geometric operations are not rigorously applicable to the p-frame. If we denote the correct DG vector (i.e., $\boldsymbol{T}^{p}_{grd}-\boldsymbol{T}^{p}_{eo}$) obtained from rigorous transformation of the point cloud after georeferencing as $\boldsymbol{T}^{p'}_{dg}$, then the direct georeferencing distortions in the p-frame can be characterized as the coordinate difference between the correct DG vector $\boldsymbol{T}^{p'}_{dg}$ and the incorrect DG vector $\boldsymbol{T}^{p}_{dg}$ .

### 2.4. Direct georeferencing distortions in national coordinates

#### 2.4.1. Datum scale distortion

For the transformation between different Cartesian frames in the same datum, the length of the DG vector always remains constant. However, according to Eq. (1), if the scale factor $m$ in the datum transformation is not equal to 1.0, then the spatial scale of the national datum will be different from the WGS 84 datum. Consequently, the distance between the ground point and the sensor center in the Cartesian frame of the national datum (e.g., e′-frame and l-frame) will be $m$ times larger than that of the WGS 84 datum, but the length of the DG vector $\boldsymbol{T}_{dg}$ computed from Eq. (10) remains unchanged. Therefore, the datum scale distortion is given by $(m-1)\boldsymbol{T}_{dg}$.

#### 2.4.2. Map projection distortions

It is rather difficult to directly identify and quantify all of the map projection distortion factors of the DG process in the p-frame, and an easier way is to analyze how to transform a DG vector from the l-frame to the p-frame. As schematically shown in Fig. 3, the transformation process involves the following four procedures:

1. Decomposition of the DG vector $\boldsymbol{T}^{l}_{dg}$ to the height component $Z_{dg}$, the horizontal distance $D$, and the horizontal angle $\phi^{l}$ (cf. Fig. 4), which here will be called "spatial observations."
2. Transformation of the "spatial observations" to the "ellipsoidal observations." $Z_{dg}$ does not need to be modified; $D$ is transformed to the geodesic distance $S$; and for the horizontal angle component, the additions of the skew-normal correction $\zeta$ and the normal-section-to-geodesic correction $\xi$ are required.
3. Transformation of the "ellipsoidal observations" to the "map-projected observations." The earth curvature correction $h_{ec}$ is added to the height component; $S$ is transformed to the projected length $D'$; and in the horizontal angle component, it needs to subtract the grid convergence $\gamma$ and to add the arc-to-chord correction $\delta$.
4. Composition of the "map-projected observations" to the DG vector $\boldsymbol{T}^{p'}_{dg}$. This is the opposite process of the first step.

The above calculation steps are very similar to the data processing procedures of the total station. The only difference is that the $Z$-axis of the total station aligns with the plumb line and therefore

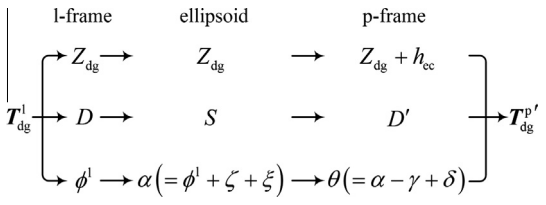


**Fig. 3.** Transformation of a DG vector from l-frame to p-frame.

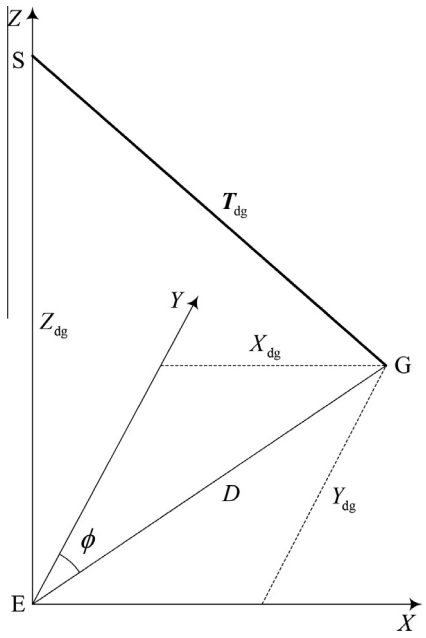


**Fig. 4.** Decomposition and composition of a DG vector. S and G represent the sensor center and the ground point, respectively. $Z_{dg}$ is the height component of the DG vector $\boldsymbol{T}_{dg}$, and $D$ and $\phi$ are the horizontal length and horizontal angle, respectively.

the gravimetric correction is required to add in its observations. As for the POS system, the inertial measurement unit (IMU) works based on the laws of Newtonian physics and its $Z$-axis aligns also with the plumb line, but the gravimetric correction is usually ignored in practice because the angular deflections are likely lower than the noise level of POS attitude data at least in case of "tactical-grade" IMUs.

According to the analysis in Section 2.2.3, the grid convergence $\gamma$ is the only difference between the angular EOPs of the l-frame and the p-frame. Therefore, if direct georeferencing is processed in the l-frame and p-frame, then their calculated DG vectors meet $\boldsymbol{T}^{p}_{dg}=\boldsymbol{R}^{p}_{l}\boldsymbol{T}^{l}_{dg}$. This means that, except for the grid convergence $\gamma$, all the other corrections added in the above procedures (i.e., the earth curvature correction $h_{ec}$, the horizontal-to-geodesic length correction $S-D$, the geodesic-to-projected length correction $D'-S$, the skew-normal correction $\zeta$, the normal-section-to-geodesic correction $\xi$, and the arc-to-chord correction $\delta$) are the map projection distortions of the direct georeferencing process in the national coordinates.

## 3. Correction of map projection distortions

The high-precision direct georeferencing in the national coordinates requires accurate correction of the datum scale distortion and the map projection distortions. As indicated in the left part of Fig. 5, the only thing to do in the datum scale correction is to multiply the DG vector $\boldsymbol{T}^{p}_{dg}$ by the datum scale factor $m$ which is usually known with sufficient accuracy. Therefore, in this section we only discuss the correction approaches of the map projection distortions.

### 3.1. High-precision approach

As schematically shown in the right part of Fig. 5, the map projection correction process for the direct georeferencing of the airborne LiDAR data is to calculate all the geometric distortions based on the DG vector and other known information (e.g., the sensor center coordinates and the map projection parameters) and to add them back directly to the DG vector. Since the decomposition

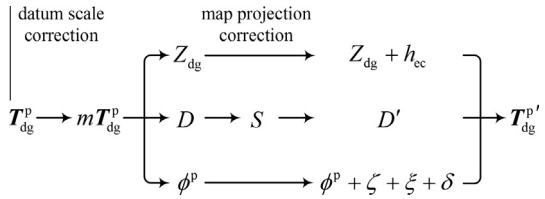


**Fig. 5.** Correction of direct georeferencing distortions in p-frame.

and composition of the DG vector only involve simple geometric operations, they are not elaborated here. In the following paragraphs, we present only the correction formulas of all the map projection distortions (except the normal-section-to-geodesic distortion $\xi$). All the formulas are directly or indirectly derived from the equations in the geometric geodesy. However, some parameters (e.g., the map projection coordinates of the ground points) in the original equations are difficult to calculate directly. Therefore, we replace them with the known values in the direct georeferencing process.

The height and length components of the map projection distortions are illustrated in Fig. 6. In the height component, only adding the earth curvature correction value is needed. Here we provide the correction equation directly, the detailed derivation is presented in Appendix B.

$$h_{ec}=\frac{D^2}{2(R_\alpha+h_S+Z_{dg})} \tag{11}$$

where $h_S$ is the ellipsoidal height of the sensor center, $R_\alpha$ is the curvature radius of the normal section in a given azimuth; and it is given by (Deakin, 2010)

$$R_\alpha=\frac{\rho\upsilon}{\rho\sin^2\alpha+\upsilon\cos^2\alpha} \tag{12}$$

where $\alpha$ is the azimuth. It can be approximately given by $\alpha=\phi^p+\gamma$, where $\phi^p$ is the horizontal angle computed from the DG vector in the p-frame.

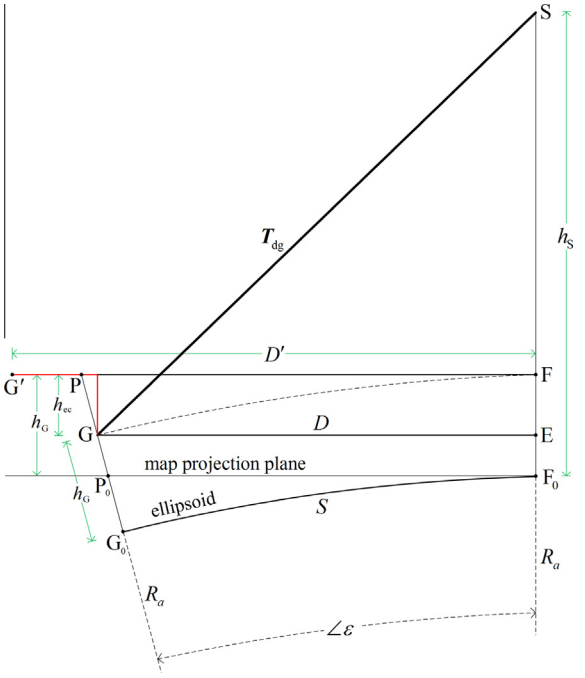


**Fig. 6.** Map projection distortions. G′ is the corresponding projected point of the ground point G (only the relative position relationship between the sensor center S and the ground point G is considered), it is not located in the SGE plane by the influence of the angle distortion.

In the length component, the first step is to calculate the geodesic distance $S$ from the horizontal length $D$. Since $S$ is always significantly shorter than the earth radius in the aerial topographic survey, the geodesic line can be approximated by the corresponding circular arc. Therefore, according to the geometric relationships in Fig. 6, we can approximately get

$$S=R_\alpha\arctan\frac{GE}{R_\alpha+SF_0-SE}=R_\alpha\arctan\frac{D}{R_\alpha+h_S+Z_{dg}} \tag{13}$$

The second step is to calculate the projected length $D'$ from the geodesic distance $S$. The equation is

$$D'=KS \tag{14}$$

where $K$ is the line scale factor. For the widely used transverse Mercator projection, it can be given by (Deakin, 2010)

$$K=k_0\left[1+\frac{X_S^2+X_SX_{G'}+X_{G'}^2}{6k_0^2R_M^2}\left(1+\frac{X_S^2+X_SX_{G'}+X_{G'}^2}{36k_0^2R_M^2}\right)\right] \tag{15}$$

where $k_0$ is the point scale factor of the central meridian, $X_S$ and $X_{G'}$ are the east coordinates (the false east is not included) of the sensor center and the ground point in the p-frame, respectively, and $R_M$ is the mean radius of curvature at the midpoint between the sensor center and the ground point. Since the ground coordinates could not be precisely acquired before the direct georeferencing, we approximately replace $X_{G'}$ and $R_M$ with $X_S+X_{dg}$ and $R$ (the mean radius of curvature at the sensor center position), respectively. Then, Eq. (15) is approximated by

$$\begin{aligned}K&=k_0\left[1+\frac{X_S^2+X_S(X_S+X_{dg})+(X_S+X_{dg})^2}{6k_0^2R^2}\left(1+\frac{X_S^2+X_S(X_S+X_{dg})+(X_S+X_{dg})^2}{36k_0^2R^2}\right)\right]\\&=k_0\left[1+\frac{3X_S^2+3X_SX_{dg}+X_{dg}^2}{6k_0^2R^2}\left(1+\frac{3X_S^2+3X_SX_{dg}+X_{dg}^2}{36k_0^2R^2}\right)\right]\end{aligned} \tag{16}$$

where $R=\sqrt{\rho\upsilon}$.

In the angle component, the skew-normal correction $\zeta$ is the horizontal included angle between the directions of the spatial straight line and its corresponding normal section (cf. Fig. 7), and it is given by (Deakin, 2010)

$$\zeta=\frac{h_G}{2\rho_M}e^2\sin(2\alpha)\cos^2\varphi_G \tag{17}$$

where $h_G$ and $\varphi_G$ are the ellipsoidal height and the geodetic latitude of the ground point, respectively, and $\rho_M$ represents the curvature radius in the meridian plane which is calculated at the midpoint position between the sensor center and the ground point. If we approximately replace $h_G$ with $h_S+Z_{dg}$, and use $\rho$ and $\varphi$ at the sensor center position, then Eq. (17) can be approximated by

$$\zeta=\frac{h_S+Z_{dg}}{2\rho}e^2\sin(2\alpha)\cos^2\varphi \tag{18}$$

The normal-section-to-geodesic distortion $\xi$ is the included angle between the directions of the normal section and the geodesic line. Given that this distortion is not numerically significant (the maximum magnitude is only on the order of 1E−9 rad) in the aerial topographic survey, there is no need for correction in the direct georeferencing process.

As shown in Fig. 8, the arc-to-chord correction is the included angle between the tangent of the projected geodesic and its corresponding chord line. For the transverse Mercator projection, it is given by (Deakin, 2010)

$$\delta=-\frac{(Y_{G'}-Y_S)(X_{G'}+2X_S)}{6k_0^2R_M^2}\left(1-\frac{(X_{G'}+2X_S)^2}{27k_0^2R_M^2}\right) \tag{19}$$

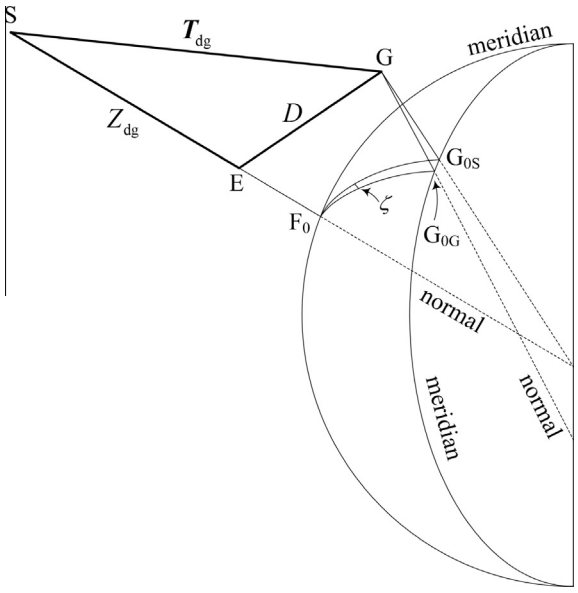


**Fig. 7.** Skew-normal correction $\zeta$. The curve $\widetilde{F_0G_{0S}}$ has the same horizontal direction as the light ray SG, and they both locate in the same plane with the normal at the sensor center S. The curve $\widetilde{F_0G_{0G}}$ is the normal section, where $G_{0G}$ is calculated by the normal at the ground point G. The angular difference between $\widetilde{F_0G_{0S}}$ and $\widetilde{F_0G_{0G}}$ is called the skew-normal correction, which is also known as the "height of target" correction because it only exists when the ground height is not zero.

where $Y_S$ and $Y_{G'}$ are the north coordinates (the false north is not included) of the sensor center and the ground point in the p-frame, respectively. Like the simplification of the line scale factor $K$ in Eq. (15), we can approximately convert Eq. (19) to

$$\delta = -\frac{Y_{dg}(3X_S + X_{dg})}{6k_0^2R^2}\left(1 - \frac{(3X_S + X_{dg})^2}{27k_0^2R^2}\right) \tag{20}$$

### 3.2. Practical approach

The high-precision correction formulas involve a lot of computational parameters and some of them (e.g., $R_\alpha$) are quite complicated, which therefore require a large amount of calculation. If the accuracy requirement is relaxed, it is necessary and convenient to use the more approximate correction equations. Although the high-precision correction formulas may have an unlimited number of approximate approaches, we only provide here our preferred simplified form.

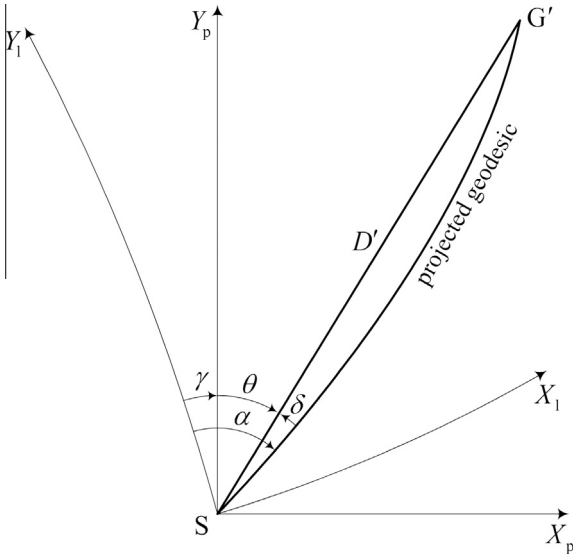


**Fig. 8.** Arc-to-chord correction $\delta$. It is the included angle between the tangent of the projected geodesic $\widetilde{SG'}$ and the straight line SG′ in the p-frame.

In the high-precision earth curvature correction equation, the calculation process of $R_\alpha$ is too complicated, and therefore we replace it with $R$. Consequently, Eq. (11) is converted into

$$h_{ec} = \frac{D^2}{2(R + h_S + Z_{dg})} \tag{21}$$

Generally, $R$ is substantially constant in a single survey area. Therefore, it can further reduce the computation amount by only using the $R$ at the center position of the survey area.

In the length component, we also use $R$ instead of $R_\alpha$, and further apply the small-angle approximation to Eq. (13) and remove the high-order terms of Eq. (16). Then, by combining these two equations, we can obtain

$$D' = \frac{k_0RD}{R + h_S + Z_{dg}}\left(1 + \frac{3X_S^2 + 3X_SX_{dg} + X_{dg}^2}{6k_0^2R^2}\right) \tag{22}$$

In the angle component, the skew-normal correction $\zeta$ can be ignored because the distortion magnitude is usually quite small, especially when the ground elevation is close to zero. As for the arc-to-chord correction $\delta$, we remove the high-order terms of Eq. (20), then

$$\delta = -\frac{Y_{dg}(3X_S + X_{dg})}{6k_0^2R^2} \tag{23}$$

Likewise, the traditional earth curvature correction and length correction equations also can be regarded as the approximation forms of the high-precision formulas. For example, in Legat's correction equations for the airborne LiDAR data (Legat, 2006), the earth curvature correction formula is given by

$$h_{ec} = \frac{D^2}{2R} \tag{24}$$

and the length correction formula is

$$D' = \left(1 - \frac{h_S + Z_{dg}}{R}\right)kD \approx \frac{kRD}{R + h_S + Z_{dg}} \tag{25}$$

where $k$ is the point scale factor of the sensor center position, and it can be given by Bomford (1980)

$$k = k_0\left(1 + \frac{X_S^2}{2k_0^2R^2} + \frac{X_S^4}{24k_0^4R^4}\right) \tag{26}$$

It can be seen by comparing Eqs. (24)–(26) to Eqs. (21)–(23) that Legat's correction formulas are different from our proposed practical formulas in three main aspects: (1) the $h_S + Z_{dg}$ term is omitted in the earth curvature correction equation; (2) the point scale factor $k$ is used to approximate the line scale factor $K$ in the length correction; and (3) the angle distortion is not considered.

## 4. Experiments

### 4.1. Accuracy evaluation

Real airborne LiDAR data are inevitably distorted by a variety of systematic and random errors (e.g., range error and atmospheric refraction), and they are very difficult to distinguish from the datum scale distortion and the map projection distortions. Therefore, only simulated data are used in this paper. The experimental process is divided into three main procedures: First, we simulate

**Table 1**
Technical characteristics of experimental national map projection frame.

| Category | Parameter | Value | Unit |
|---|---|---|---|
| Helmert 7-parameter | $m$ | 1.00005 | – |
| | $(X, Y, Z)$ | (370.9492, 282.6227, −4.7778) | m |
| | $(\omega, \varphi, \kappa)$ | (−0.0014, 0.0022, −0.0025) | deg |
| Ellipsoid | Type | Krassovsky | – |
| Map projection | Type | universal transverse Mercator | – |
| | Central meridian | 117 | deg |

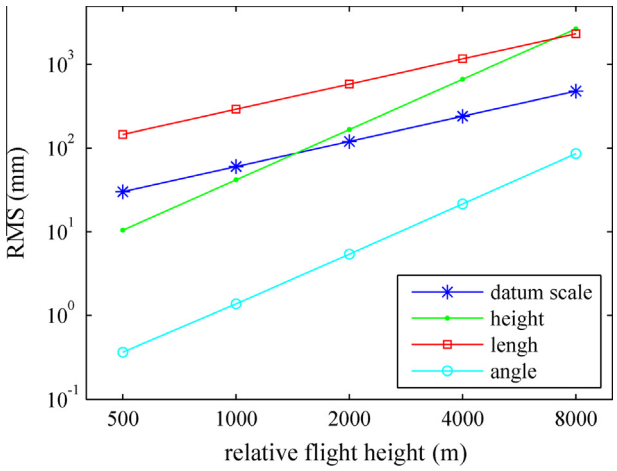


**Fig. 9.** Magnitudes of different direct georeferencing distortions in p-frame.

the laser scanning observations and trajectory data and further transform the latter to the e-frame and p-frame. In the second step, we perform the direct georeferencing process in the e-frame, then transform the ground points to the geodetic coordinates of the national datum and further project them to the required p-frame. The used transverse Mercator projection algorithm comes from the GeographicLib library, which is an open source geographic coordinate conversion library developed by Karney (2013). According to the test results by Karney (2011), the maximum error of our used map projection formula is only a few nanometers. Therefore, the direct georeferencing results of the e-frame can be treated as the true values. In the third step, we perform the direct georeferencing process in the p-frame and compensate the datum scale distortion and the map projection distortions by using different correction schemes. Then, the calculated ground points are compared with their true values, and the coordinate differences are the direct georeferencing residuals in the national coordinates.

To verify the correctness of the proposed map projection distortions model, the basic experimental strategy is to simulate the adverse survey condition as far as possible. Table 1 shows the definition of the national map projection frame, which comes from a real case of aerial photogrammetric project. The geodetic coordinate of the laser emission center is (30°N, 120°E), and therefore the longitude difference is 3°. A hypothetical scanner-less frame imaging LiDAR system with a field of view (FOV) of approximately $73.86° \times 73.86°$ is employed, which aims to simulate the imaging coverage area of a Leica RC-30 camera. Five datasets with different relative flight heights are simulated, where the minimum and maximum values are 500 m and 8000 m, respectively. Every dataset includes a total of $11 \times 11$ ground points, and they are evenly distributed within the imaging coverage area. All ground points have the same ellipsoidal height of 1000 m.

Fig. 9 schematically shows the magnitudes of the datum scale distortion and the map projection distortions in the elevation, length, and angle components. Under the experimental conditions of this paper, the length distortion is much larger than the other three parts in almost all the scenarios. The height distortion significantly increases with the increasing flight height because, according to Eq. (21), it is a quadratic function of the horizontal length $D$; whereas the datum scale distortion and the length distortion (cf. Eq. (22)) only linearly grow with the length and the horizontal length of the DG vector, respectively. As for the angle distortion, the magnitude is usually very small, especially when the relative flight height is lower than 2000 m.

Table 2 presents the error statistics of different direct georeferencing correction schemes in the p-frame. It can be seen that most distortions can be compensated by Legat's map projection correction formulas, but the residuals are still significant in all scenarios. When the relative flight height is low (500 m), almost all of the residuals come from the datum scale distortion. The residuals in the height component are constant, which is due to the fixed ground heights in the simulated data. When the relative flight height is very high (8000 m), the correction residuals of the map projection distortions should also not be ignored, and they mainly appear in the plane component. Our proposed high-precision

**Table 2**
Error statistics of different correction schemes.

| Relative flight height | Datum scale correction | Map projection correction | Mean (mm) | | Std. dev. (mm) | | Max. dev. (mm) | |
|---|---|---|---|---|---|---|---|---|
| | | | Plane | Height | Plane | Height | Plane | Height |
| 500 m | No | No | 152.9 | 16.1 | 56.9 | 5.6 | 258.6 | 25.0 |
| | No | Legat | 15.8 | 25.0 | 5.9 | 0.0 | 27.3 | 25.0 |
| | Yes | Legat | 0.4 | 0.0 | 0.3 | 0.0 | 1.2 | 0.0 |
| | Yes | Practical | 0.2 | 0.0 | 0.1 | 0.0 | 0.3 | 0.0 |
| | Yes | High-precision | 0.0 | 0.0 | 0.0 | 0.0 | 0.0 | 0.0 |
| 2000 m | No | No | 611.7 | −41.9 | 227.7 | 89.0 | 1043.2 | −254.9 |
| | No | Legat | 63.2 | 100.0 | 24.2 | 0.2 | 118.4 | 100.5 |
| | Yes | Legat | 6.5 | 0.0 | 4.1 | 0.2 | 17.0 | 0.5 |
| | Yes | Practical | 0.6 | 0.0 | 0.3 | 0.2 | 1.1 | −0.4 |
| | Yes | High-precision | 0.0 | 0.0 | 0.0 | 0.0 | 0.0 | 0.0 |
| 8000 m | No | No | 2446.8 | −1871.1 | 914.9 | 1424.2 | 4313.5 | −5278.4 |
| | No | Legat | 263.6 | 400.2 | 131.7 | 3.6 | 634.1 | 407.4 |
| | Yes | Legat | 103.3 | 0.4 | 64.8 | 3.6 | 263.2 | 7.7 |
| | Yes | Practical | 2.7 | 0.0 | 1.2 | 3.6 | 5.6 | −7.2 |
| | Yes | High-precision | 0.1 | 0.0 | 0.0 | 0.0 | 0.2 | 0.0 |

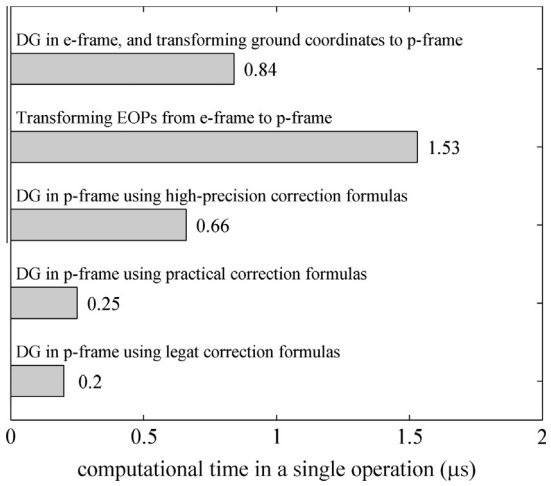


**Fig. 10.** Computational costs of different data processing procedures. The test program ran on a 2.13 GHz Intel processor and was compiled with the Intel C/C++ compiler (version 12.0).

correction approach can compensate almost all direct georeferencing distortions in the p-frame even for the extreme case of 8000 m flight height above ground, and the correction accuracy of the practical approach is only slightly worse.

### 4.2. Computational performance

Computational efficiency is also a very important issue to evaluate the performance of different direct georeferencing approaches. For the direct georeferencing in the e-frame, it requires the transformation of all ground points from e-frame to p-frame. The map projection is the most time-consuming operation, and it depends largely on the map projection type and the specific algorithm used. After careful testing two transverse Mercator projection formulas (i.e., USGS formula and JHS formula) from (International Association of Oil and Gas Producers, 2013) and two algorithm implementations from the GeographicLib library (Karney, 2013), we finally chose USGS formula in our experiment due to its lowest computational cost. As for the direct georeferencing in the p-frame, it first requires transforming the EOPs from e-frame to p-frame, and then performing the direct georeferencing in the p-frame and the compensation of various geometric distortions. The linear EOPs were also transformed by the USGS formula, and the angular EOPs conversion formulas came from Section 2.2.

As shown in Fig. 10, the single operation of transforming the EOPs from e-frame to p-frame requires several times more time than other calculation procedures. However, the typical measurement frequency of airborne POS data is only a few hundred Hz, whereas the pulse repetition frequencies (PRF) of the state-of-the-art commercial airborne LiDAR systems (Petrie, 2011) are up to 50–500 kHz. Therefore, the consumed time for transforming the EOPs is almost negligible when compared to the correction process of the map projection distortions. All of the three p-frame DG schemes which use different map projection correction formulas require less computational effort than the DG approach in the e-frame. Legat's correction method has the lowest computational cost, and it can save about 76% of time compared to the transformation of the ground points. Our proposed practical map projection correction approach is slower than the Legat's method by about 25%, whereas the high-precision correction approach is much slower.

### 4.3. Discussion

After evaluating the computational accuracies and efficiencies of different correction schemes, our recommendations for the theoretical and practical applications are as follows:

1. The datum scale correction is always required, but luckily it is very easy to perform.
2. The accuracy of Legat's map projection correction formulas can meet the requirements of most aerial LiDAR data because currently, most commercial airborne LiDAR systems operate below 3000 m flight height (Petrie, 2011).
3. The practical map projection correction formulas can be used in the direct georeferencing process of high-altitude aerial imagery. But the correction algorithm should be reformulated because the DG vector could not be directly acquired in the photogrammetry.
4. The high-precision map projection correction approach is primarily of theoretical, rather than practical interest. It proves the validity of our proposed map projection distortions model, and it also can be used to evaluate the accuracies of different GPS/INS attitude transformation methods to the p-frame (Bäumker and Heimes, 2002; Legat, 2006; Zhao et al., 2013).

## 5. Conclusions

In this paper, all of the major geometric distortion factors in the georeferencing process of the national coordinates were identified and properly modeled. According to our analysis, one datum scale distortion and a total of six map projection distortion factors exist, the latter of which can be further divided into three categories: (1) the elevation component which includes the earth curvature distortion; (2) the length component which includes the horizontal-to-geodesic length distortion and the geodesic-to-projected length distortion; and (3) the angle component which includes the skew-normal distortion, the normal-section-to-geodesic distortion, and the arc-to-chord distortion. Accordingly, two groups of map projection correction formulas, i.e., the high-precision formulas and the practical formulas, are derived to address the theoretical and practical applications.

The simulated experiments show that the datum scale distortion is numerically significant in all conditions of the testing flight heights, and it should always be corrected. The high-precision map projection correction formulas can compensate almost all map projection distortions even under the extreme condition with the relative flight height of 8000 m, which proves the correctness of our proposed map projection distortions model. In the experimental scenario with the relative flight height of 2000 m, the maximum error of Legat's map projection correction approach is only about 1.7 cm, and therefore it is suitable for the direct georeferencing of airborne LiDAR data with medium and low flying height. Our proposed practical correction approach is a little slower than Legat's approach by about 25%, but the correction accuracy is much better in the high flight height scenario. It can be useful for the direct georeferencing process of the high-altitude aerial imagery.

## Acknowledgements

This work was supported in part by the National Natural Science Foundation of China Grant 41171292, and the National Hi-Tech Research and Development Program Grant 2013AA12A401. The authors would also like to thank Charles F.F. Karney for his contribution on GeographicLib.

## Appendix A. Notation

The following symbols are used in this paper:

| Category | Symbol | Meaning |
|---|---|---|
| Reference frame | s | Sensor frame |
| | e | Earth-centered earth-fixed frame |
| | e′ | Eccentric earth-fixed frame |
| | l | Local level frame of the national ellipsoid |
| | p | Map projection frame |
| Spatial position | S | Sensor center |
| | G | The ground point in a Cartesian frame |
| | G′ | The ground point in the map projection frame |
| Variable | $\boldsymbol{T}$ | 3D vector or coordinate |
| | $\boldsymbol{R}$ | $3 \times 3$ Rotation matrix |
| | $\varphi$ | Geodetic latitude |
| | $\lambda$ | Geodetic longitude |
| | $\lambda_0$ | The geodetic longitude of the central meridian |
| | $h$ | Ellipsoidal height |
| | $h_{ec}$ | Earth curvature correction |
| | $e$ | The first eccentricity of the ellipsoid |
| | $\rho$ | The curvature radius in the meridian plane |
| | $\upsilon$ | The curvature radius in the prime vertical plane |
| | $R_\alpha$ | The curvature radius of the normal section in a given azimuth |
| | $R$ | The mean radius of curvature |
| | $m$ | Datum scale factor |
| | $K$ | Line scale factor |
| | $k$ | Point scale factor |
| | $k_0$ | The point scale factor of the central meridian |
| | $D$ | The horizontal length of the DG vector |
| | $D'$ | The projected length of the DG vector |
| | $S$ | Geodesic distance |
| | $\alpha$ | Azimuth |
| | $\gamma$ | Grid convergence |
| | $\zeta$ | Skew-normal correction |
| | $\xi$ | Normal-section-to-geodesic correction |
| | $\delta$ | Arc-to-chord correction |
| | $\phi$ | The horizontal angle of the DG vector |
| | $\theta$ | Plane bearing |

## Appendix B. Derivation of earth curvature correction equation

As schematically shown in Fig. 6, the earth curvature correction $h_{ec}$ is the height difference between the ground point G in a Cartesian frame of the national datum and the corresponding projected ground point G′. Given that the horizontal length of the DG vector is always far shorter than the earth radius, G and F can be approximately regarded as locating at a same arc with the radius $(R_\alpha + h_G)$. If we denote O as the ellipsoid center, we can then obtain

$$h_{ec} = \cos\varepsilon \cdot GP = \cos\varepsilon(\sec\varepsilon \cdot OF - OG) = (1-\cos\varepsilon)(R_\alpha + h_G) \approx \frac{1}{2}\varepsilon^2(R_\alpha + h_G) \quad (B1)$$

where $\varepsilon$ is the central angle in radians. According to the geometric relationship in Fig. 6, it can be given by

$$\varepsilon = \arctan\left(\frac{GE}{R_\alpha + SF_0 - SE}\right) = \arctan\left(\frac{D}{R_\alpha + h_S + Z_{dg}}\right) \approx \frac{D}{R_\alpha + h_S + Z_{dg}} \quad (B2)$$

where $Z_{dg}$ is the height component of the DG vector, and it is always negative. Submitting Eq. (B2) into Eq. (B1), we can finally get

$$h_{ec} = \frac{D^2}{2(R_\alpha + h_S + Z_{dg})^2}(R_\alpha + h_G) = \frac{D^2}{2(R_\alpha + h_S + Z_{dg})^2}(R_\alpha + h_S + Z_{dg} + h_{ec}) \approx \frac{D^2}{2(R_\alpha + h_S + Z_{dg})} \quad (B3)$$

## References


Bäumker, M., Heimes, F.J., 2002. New calibration and computing method for direct georeferencing of image and scanner data using the position and angular data of an hybrid inertial navigation system. In: Heipke, C., Jacobsen, K., Wegmann, H. (Eds.), Integrated Sensor Orientation-Test Report and Workshop Proceedings, vol. 43. OEEPE Official Publication, Hannover, pp. 197–212.

Blázquez, M., Colomina, I., 2012. Relative INS/GNSS aerial control in integrated sensor orientation: models and performance. ISPRS Journal of Photogrammetry and Remote Sensing 67 (1), 120–133.

Bomford, G., 1980. Geodesy, fourth ed. Clarendon Press, Oxford.

Deakin, R.E., 2010. Traverse Computation on the Ellipsoid and on the Universal Transverse Mercator Projection. <http://user.gs.rmit.edu.au/rod/files/publications/Trav_Comp_V2.1.pdf> (accessed 03.07.13).

Habib, A., Pullivelli, A., Mitishita, E., Ghanma, M., Kim, E.M., 2006. Stability analysis of low-cost digital cameras for aerial mapping using different georeferencing techniques. Photogrammetric Record 21 (113), 29–43.

Hothmer, J., 1958. Possibilities and limitations for elimination of distortion in aerial photographs. Photogrammetric Record 2 (12), 426–445.

International Association of Oil and Gas Producers, 2013. Coordinate Conversions and Transformations Including Formulas. <http://www.epsg.org/guides/docs/G7-2.pdf> (accessed 03.07.13).

Ip, A., El-Sheimy, N., Mostafa, M., 2007. Performance analysis of integrated sensor orientation. Photogrammetric Engineering & Remote Sensing 73 (1), 89–97.

Karney, C.F.F., 2011. Transverse Mercator with an accuracy of a few nanometers. Journal of Geodesy 85 (8), 475–485.

Karney, C.F.F., 2013. GeographicLib. <http://geographiclib.sourceforge.net/> (accessed 03.07.13).

Khoshelham, K., 2009. Role of tie points in integrated sensor orientation for photogrammetric map compilation. Photogrammetric Engineering & Remote Sensing 75 (3), 305–311.

Legat, K., 2006. Approximate direct georeferencing in national coordinates. ISPRS Journal of Photogrammetry and Remote Sensing 60 (4), 239–255.

Petrie, G., 2011. Current developments in the technology airborne topographic laser scanners. GeoInformatics 1–2, 34–44.

Redfearn, J.C.B., 1948. Transverse Mercator formulae. Survey Review 9 (69), 318–322.

Ressl, C., 2001. The impact of conformal map projections on direct georeferencing. International Archives of Photogrammetry Remote Sensing and Spatial Information Sciences 34 (Part B), 283–288.

Skaloud, J., 2002. Direct georeferencing in aerial photogrammetric mapping. Photogrammetric Engineering & Remote Sensing 68 (3), 207–210.

Skaloud, J., Legat, K., 2008. Theory and reality of direct georeferencing in national coordinates. ISPRS Journal of Photogrammetry and Remote Sensing 63 (2), 272–282.

Wang, S.C., 1980. Einfluß der geodätischen Abbildungsverzerrungen auf die photogrammetrische Punktbestimmung. Ph.D. thesis, Deutsche Geodätische Kommission, München, Germany, 162p (in German).

Yastikli, N., Jacobsen, K., 2005. Direct sensor orientation for large scale mapping—Potential, problems, solutions. Photogrammetric Record 20 (111), 274–284.

Zhao, H., Zhang, B., Wu, C., Zuo, Z., Chen, Z., 2013. Development of a Coordinate Transformation method for direct georeferencing in map projection frames. ISPRS Journal of Photogrammetry and Remote Sensing 77, 94–103.